Appl. Phys. B 47, 343–348 (1988)

Applied Physics B Photophysics and Laser Chemistry

Quantitative Analysis of Photoacoustic IR Spectra

J. Brunn, P. Grosse, and R. Wynands

I. Physikalisches Institut der Rheinisch-Westfälischen Technischen Hochschule, D-5100 Aachen, Fed. Rep. Germany

Received 16 February 1988/Accepted 9 June 1988

Abstract. Photoacoustic spectroscopy is a method for directly measuring the absorption properties of gases and condensed matter. We have developed a photoacoustic gas cell for a rapid-scan Fourier spectrometer. With this cell we can extend the spectral range down to 180 cm^{-1}; more than one octave lower than previously reported useful broadband measurements. The photoacoustic spectrum of a microscope cover glass was measured from 180 ... 2000 cm^{-1} and normalized with respect to the spectrum of carbon black as a reference material. Starting from the one-dimensional equation of heat conduction we derived an expression for the surface temperature of single and double-layer samples. We calculated the surface temperature of the glass lamella and divided it by the corresponding values for carbon black using the thermal conductivity of carbon black as a fitting parameter. We show that the one-dimensional model calculation reproduces the experimental spectrum over the whole spectral range.

PACS: 07.65, 07.65G, 78.30

In photoacoustic spectroscopy (PAS) light from an intensity-modulated light source falls through a window onto a sample at the bottom of a sealed gas cell. The sample is heated by Joule's heat due to the optical absorption. According to a model developed by Rosencwaig and Gersho [1] the heat is partially transferred to the sample surface from where the gas is heated up within a small boundary layer (typically 1–2 mm thick depending on the modulation frequency). This layer expands periodically and compresses the rest of the gas volume adiabatically like a piston causing pressure variations which can be detected by a sensitive microphone attached to the cell. A recent and comprehensive overview on photoacoustic spectroscopy may be found in [2].

In their treatment Rosencwaig and Gersho assume the special case of an exponential decrease of absorbed light intensity inside the sample (Lambert-Beer-law). In the case of transparent samples, however, which might exhibit optical interference effects or in the case of a light scattering sample, the exponential law no longer holds. Thus, many authors extended this simple model with respect to interference effects and multilayer structures.

In 1978 the applicability of photoacoustics to Fourier transform IR spectroscopy was demonstrated for the first time by Busse and Bullemer [3]. The multiplex and throughput advantages reduce the noise problems due to the low luminosity of thermal light sources in the far infrared regime.

In the following we mention briefly how the spectral range was extended into the FIR regime. We show that photoacoustic spectra can be simulated using an extended one-dimensional theory. By adjusting the thermal conductivity of carbon black, an absolute calibration of simulated spectra is possible.

1. Experimental Setup

1.1. The Spectrometer

We used a Bruker rapid-scan Fourier spectrometer model IFS 114. In a Fourier spectrometer, light is modulated by moving the mirrors of a Michelson interferometer in such a way that the optical path difference between the two beams is varied with constant speed v_m. Light of wavenumber $\tilde{\nu}$ is then

modulated with

$\omega = 2\pi\tilde{\nu}v_m$.

This means that in contrast to lock-in techniques a broad range of modulation frequencies has to be processed. This must be taken into special consideration when designing a photoacoustic cell.

1.2. The Cell

We developed a PAS cell which can be operated down to 180 cm^{-1}. In conventional setups the lower end of the frequency range used to be at 400 cm^{-1} [4]. The background absorption of the empty cell is substantially lower than 1% compared to the photoacoustic signal of carbon black as a totally absorbing reference sample.

Since we wanted to use our cell in a Fourier spectrometer – i.e. with a broad band of modulation frequencies – we designed the cell to have no resonances inside the frequency range typically used in the measurements (20–500 Hz). The frequency characteristic remains flat up to about 1000 Hz, and a weak and broad resonance peak can be observed at about 2300 Hz.

Acoustic noise from the surroundings is suppressed very efficiently so that useful measurements have been possible down to 180 cm^{-1}. To avoid sound coupling via the air we designed the cell to be vacuum proof, so it can be used in the evacuable sample chamber of our spectrometer. To suppress impact sound and sound transmitted by solids the cell is mounted in a spring-buffered frame. The spectrometer itself is insulated by so-called "stop-chocs".

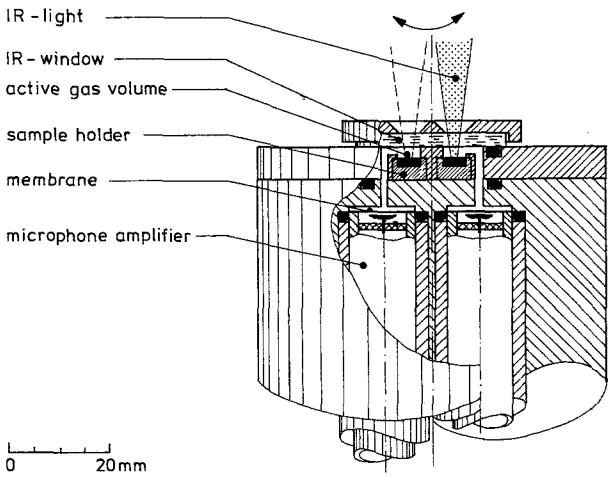

Fig. 1. Schematic diagram of the photoacoustic cell which consists of two sample chambers. A mirror above the detector switches the light between the two samples. The cell is vacuum proof so that it can be placed in an evacuable spectrometer. Interfering sound transmitted by air can be suppressed completely. This arrangement allows difference measurements between the two halves of the cell

Our cell has two independent sample chambers, each containing one condenser microphone (Bruel & Kjær type 4166) (Fig. 1). This construction allows us to obtain the spectra of the sample and a reference material without having to break the vacuum or open the cell. For this purpose a mirror which can be operated from outside the spectrometer switches the incident light beam between the two halves of the cell.

Due to the high sensitivity of photoacoustic spectroscopy, water absorption bands are always a problem in IR measurements. We reduce this nuisance by filling the cell with dry helium. But water desorbing from the cell walls during the experiment leads to an additional photoacoustic signal. The resulting peaks in the spectra are suppressed by subtracting data obtained with an empty cell.

1.3. The Measurements

For all the measurements we filled the cell with dry helium and chose brass with a thin gold coating as backing material. Gold has a reflectance of 100% in the IR and so ensures that no light is absorbed by the backing.

The cell window (CsI) has a transmittance of about 90% in the spectral regime from 180 cm^{-1} to higher wavenumbers.

We always use carbon black as our reference material since this powder has an absorbance of 100% in the spectral regime of interest. Figure 2 shows a typical carbon black spectrum. The overall structure and the dips reflect the characteristics of the spectrometer. The ratio of two such spectra gives a 100% line which means that the spectra are well reproducible.

2. Numerical Simulation

2.1. Temperature at the Sample Surface

We consider the system sketched in Fig. 3. The system of layers and the incident light are assumed to be invariant against translation in a direction perpendicular to the incident light. Although in our cell the sample has a diameter of 5 mm we shall see below that such a one-dimensional treatment is sufficient to describe the measured spectra. Each layer is characterized by the following quantities:

ϱ_j: mass density
c_j: mass specific heat capacity
λ_j: thermal conductivity
$\varepsilon_j(\tilde{\nu})$: dielectric function
$\sqrt{\varepsilon_j} = n_j + i\kappa_j$: complex index of refraction

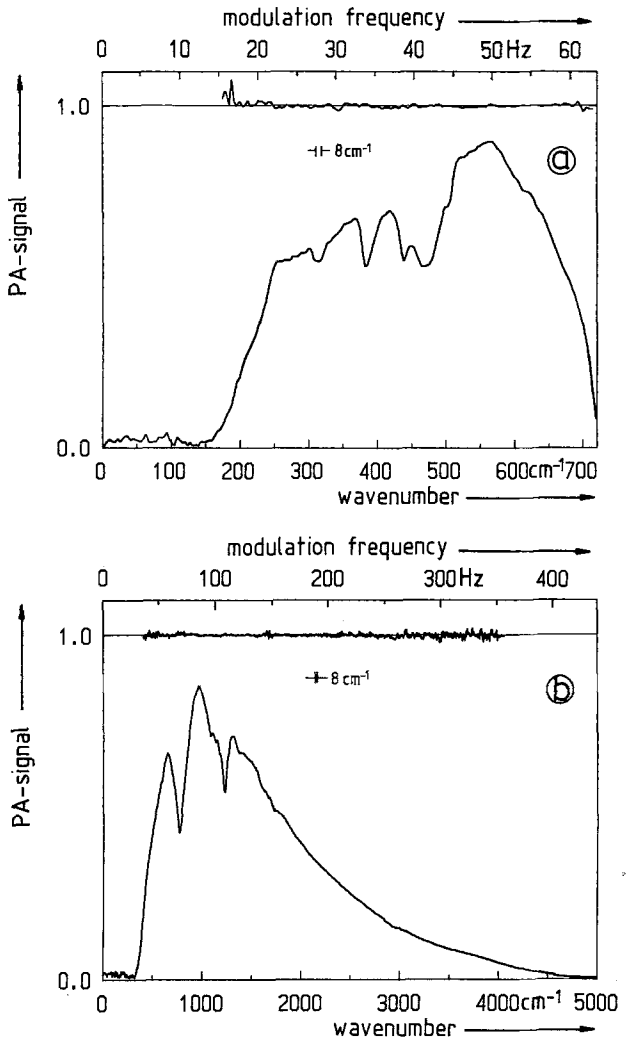

Fig. 2a, b. Carbon black reference spectrum. The 100% line is the ratio of two reference spectra. The noise level is less than 1%. (a) Interferometer equipped for the spectral range from 180–700 cm^{-1} (64 scans, $v_m = 0.88$ mm/s). (b) Interferometer equipped for the spectral range from 400–4000 cm^{-1} (32 scans, $v_m = 0.88$ mm/s)

where the index j denotes the layers 0 ... 3. We assume all these quantities to be constant within the respective layers. The resulting one-dimensional equation of heat conduction describing the balance between the local heating and the resulting heat flux in layer j reads

$$\lambda_j \frac{\partial^2 \theta_j(z,t)}{\partial z^2} - \varrho_j c_j \frac{\partial \theta_j(z,t)}{\partial t} = -p(z,t), \tag{1}$$

where $\theta_j(z,t)$ is the oscillatory part of the temperature and $p(z,t)$ the density of absorbed power.

Since the incident light beam is modulated, $p(z,t)$ is modulated, too:

$$p(z,t) = Q(z) \cdot I_0 \exp(-i\omega t),$$

$\omega \equiv$ modulation frequency.

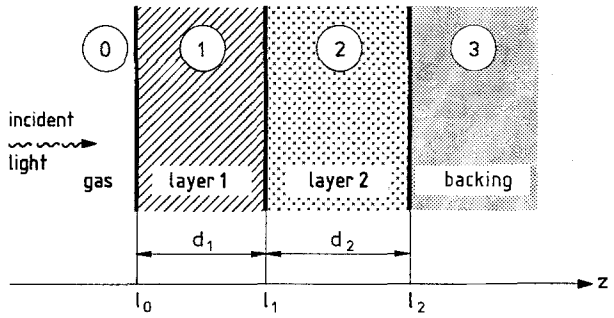

Fig. 3. Schematic diagram of the layer system considered in the numerical simulations

Here $I_0 Q(z)$ is the spatial distribution of heat sources, i.e. that portion of the intensity of the incident light beam which is absorbed at position z. For $Q(z)$, an arbitrary distribution can be considered; we only need to demand that certain integrals involving $Q(z)$ (see below) converge; this is fulfilled if $Q(z)$ is finite.

Setting the stationary solution

$$\theta_j(z,t) = T_j(z) \exp(-i\omega t)$$

in (1) yields:

$$\frac{d^2 T_j(z)}{dz^2} - \gamma_j^2 T_j(z) = -\frac{I_0 Q(z)}{\lambda_j} \tag{2}$$

with the abbreviation $\gamma_j = (-1+i)\sqrt{\frac{\omega \varrho_j c_j}{2\lambda_j}}$. The quantity $\mu_{\text{therm}} = \sqrt{\frac{2\lambda_j}{\omega \varrho_j c_j}}$ is called the thermal diffusion length inside layer j at modulation frequency ω and is the thermal analogue to the optical penetration depth $d_{\text{opt}} = \frac{1}{K}$ where K is the optical absorption constant. The general solution of (2) is

$$\begin{aligned} T_j(z) = {} & A_j \exp[\gamma_j(z - l_{j-1})] \\ & + B_j \exp[-\gamma_j(z - l_{j-1})] \\ & + \frac{I_0}{2\lambda_j \gamma_j} \Big\{ \exp[-\gamma_j(z - l_{j-1})] \\ & \times \int_{l_{j-1}}^{l_j} Q(\xi) \exp[\gamma_j(\xi - l_{j-1})] d\xi \\ & - \exp[\gamma_j(z - l_{j-1})] \\ & \times \int_{l_{j-1}}^{l_j} Q(\xi) \exp[-\gamma_j(\xi - l_{j-1})] d\xi \Big\}, \end{aligned}$$

where l_j and l_{j-1} are defined as in Fig. 3 and $l_{-1} = -\infty$, $l_3 = \infty$.

Using $Q(z) = 0$ for $z < l_0$ and for $z > l_2$ and the set of boundary conditions (continuity of temperature and

heat flux)

$$T_0(-\infty)=0, \quad T_3(\infty)=0,$$

$$T_0(l_0)=T_1(l_0), \quad \lambda_0\frac{dT_0}{dz}\bigg|_{z=l_0}=\lambda_1\frac{dT_1}{dz}\bigg|_{z=l_0},$$

$$T_1(l_1)=T_2(l_1), \quad \lambda_1\frac{dT_1}{dz}\bigg|_{z=l_1}=\lambda_2\frac{dT_2}{dz}\bigg|_{z=l_1},$$

$$T_2(l_2)=T_3(l_2), \quad \lambda_2\frac{dT_2}{dz}\bigg|_{z=l_2}=\lambda_3\frac{dT_3}{dz}\bigg|_{z=l_2},$$

we have a system of eight linear equations for A_0, A_1, A_2, A_3, B_0, B_1, B_2, B_3. We want to calculate the temperature at the sample surface $T_0(l_0)$. Solving the equations yields

$$T_0(l_0)=\frac{I_0X_1}{\lambda_1\gamma_1X_2}, \tag{3}$$

$$\begin{aligned}X_1=&[(g_{12}+1)(1+g_{32})\exp(-\gamma_2d_2)\\&+(g_{12}-1)(1-g_{32})\exp(\gamma_2d_2)]\\&\times\exp(-\gamma_1l_1)\int_{l_0}^{l_1}Q(\xi)\exp(\gamma_1\xi)d\xi\\&+[(g_{12}+1)(1-g_{32})\exp(\gamma_2d_2)\\&+(g_{12}-1)(1+g_{32})\exp(-\gamma_2d_2)]\\&\times\exp(\gamma_1l_1)\int_{l_0}^{l_1}Q(\xi)\exp(-\gamma_1\xi)\mathrm{d}\xi\\&+2g_{12}\Bigg[(1+g_{32})\exp(-\gamma_2l_2)\int_{l_1}^{l_2}Q(\xi)\exp(\gamma_2\xi)d\xi\\&+(1-g_{32})\exp(\gamma_2l_2)\int_{l_1}^{l_2}Q(\xi)\exp(-\gamma_2\xi)d\xi\Bigg],\end{aligned}$$

$$\begin{aligned}X_2=&(g_{12}+1)[(1-g_{01})(1-g_{32})\exp(\gamma_2d_2+\gamma_1d_1)\\&-(1+g_{01})(1+g_{32})\exp(-\gamma_2d_2-\gamma_1d_1)]\\&+(g_{12}-1)[(1-g_{01})(1+g_{32})\exp(-\gamma_2d_2+\gamma_1d_1)\\&-(1+g_{01})(1-g_{32})\exp(\gamma_2d_2-\gamma_1d_1)],\end{aligned}$$

where $g_{jk}=\sqrt{\frac{\varrho_jc_j\lambda_j}{\varrho_kc_k\lambda_k}}$.

For a sample consisting of one layer only ($\lambda_1=\lambda_2$, $\gamma_1=\gamma_2$, $\varepsilon_1=\varepsilon_2$) Eq. (3) reduces to

$$T_0(l_0)=\frac{I_0}{\lambda_S\gamma_S}\frac{(1-g_{3S})\exp(-\gamma_Sl_2)\int_{l_0}^{l_2}Q(\xi)\exp(\gamma_S\xi)d\xi+(1+g_{3S})\exp(\gamma_Sl_2)\int_{l_0}^{l_2}Q(\xi)\exp(-\gamma_S\xi)d\xi}{(1+g_{3S})(1+g_{0S})\exp(\gamma_Sd_S)-(1-g_{3S})(1-g_{0S})\exp(-\gamma_Sd_S)}, \tag{4}$$

where the index S refers to the sample layer. This formula was derived using a different approach by Afromowitz et al. [5].

2.2. The Distribution of Heat Sources

$Q(z)$ in the previous formulas denotes the density of the absorbed power at position z, divided by the intensity of the beam incident onto the sample surface. For non-magnetic homogeneous materials we get $Q(z)$ for $l_{j-1}<z\leqq l_j$ from [6]:

$$Q(z)=-\frac{\langle\nabla\mathbf{S}\rangle}{\langle S_z\rangle}=\frac{2\pi\tilde{\nu}\,\mathrm{Im}\{\varepsilon_j\}}{n_0}\left|\frac{E_j(z)}{E_0}\right|^2$$

$\mathbf{S}$: Poynting vector
S_z: component of the Poynting vector in z-direction
E_0: amplitude of the electric field of the wave incident onto the sample
$E_j(z)$: amplitude of the electric field at position z inside layer j.

$E_j(z)/E_0$ for the two sample layers can be obtained by considering the optics of the multi-layer structure "cell and sample". As an extension to the treatment of Rosencwaig and Gersho we can account for optical multiple interference effects between the sample layers and the backing material by using the matrix method described in [7]. The distance from the cell window to the sample surface is about 2 mm, so we neglect any interference effects between these two surfaces because the experimental resolution is usually less than the distance of these interference structures.

2.3. The Photoacoustic Signal

It is easily seen from Rosencwaig and Gersho's results that the smaller the gas volume, the larger the signal amplitude [1]. But a small gas volume – as is the case in our cell – means that for low frequencies (where μ_{therm} is large) the gas piston's size is comparable to the total gas length. This is in contradiction to Rosencwaig and Gersho's model which requires the gas layer to be thin in comparison to the gas length. But if this is no longer the case we cannot expect the pressure amplitude Rosencwaig and Gersho derived to be correct.

The analysis we present here doesn't require a detailed knowledge of the process of signal generation, but instead we calculated the temperature amplitude of the sample surface and compared it with the calculated surface temperature amplitude for carbon black. Assuming that the acoustic signal is proportional to the surface temperature, this eliminated the difficulties which arise if one tries to describe the signal generation within the gas quantitatively.

In Sect. 3.2 we shall discuss how the thermal and optical properties of carbon black can be determined. After inserting these values into formula (4) we ob-

tained a simulated carbon black spectrum which we used to calibrate the simulated sample spectra.

3. Results and Discussion

3.1. Glass Lamella

One sample we studied was a glass lamella of thickness 135 μm – a microscope cover glass. Density, specific heat capacity, and thermal conductivity of our glass sample were taken from literature, and the thickness was measured by an inductive measurement tool. The dielectric function ε was obtained from reflectance (R) and transmittance (T).

a) R and T (Fig. 4) were measured with our Fourier spectrometer. Under the condition that $n \gg \kappa$ – which is fulfilled for glass – and if no Fabry-Perot-fringes occur in the spectra it is possible to express R and T by the following approximations:

$$R = R_\infty (1 + T\exp(-2k_0\kappa d)),$$
$$T = \frac{(1-R_\infty)^2 \exp(-2k_0\kappa d)}{1-R_\infty^2 \exp(-4k_0\kappa d)}, \tag{5}$$

with

$$R_\infty = \frac{(n-1)^2+\kappa^2}{(n+1)^2+\kappa^2}.$$

If the thickness d of the sample is known (5) can be solved to obtain n and κ – at least as long as T is not too small. The interference fringes, which can be seen in the spectra of the glass sample (Fig. 4), were suppressed by reducing the experimental resolution. This could be done very easily by restricting the length of our interferogram before Fourier transforming it.

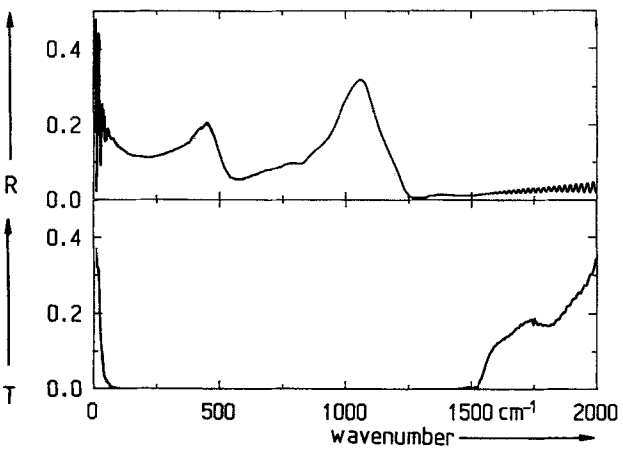

Fig. 4. Reflectance and transmittance of the microscope cover glass (thickness 135 μm)

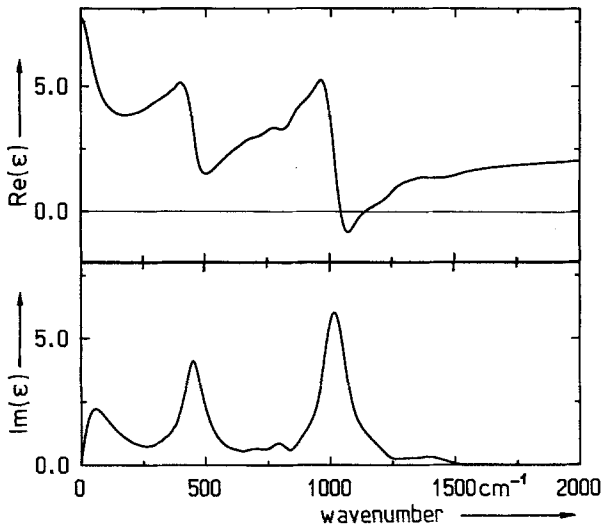

Fig. 5. Dielectric function ε of the glass sample. The curves were obtained by the methods described in the text

b) In the spectral regime where glass is no longer transparent we used a Kramers-Kronig-transformation to get the phase of R. Then ε is easily obtained.

Figure 5 shows the resulting ε for our glass sample. The perceived structures are due to the four eigenmodes of the SiO_4 tetrahedrons [8]. These data of ε were used for further calculations.

Figure 6a shows the result of the photoacoustic experiment for the glass sample, normalized with respect to a measured carbon black spectrum. In the same frame the simulated spectrum is given, after dividing by a calculated carbon black spectrum. The quantitative agreement between experiment and simulation above 400 cm^{-1} indicates that the assumptions made to carry out the simulation are justified. Specifically, it is sufficient to use a one-dimensional model of our PA cell without any detailed knowledge about what happens within the gas volume.

Since we did not press the sample onto the backing, it "floated" on a thin helium layer. In our simulation we took such a discontinuity in the temperature field into account by introducing a helium film of thickness 10 μm between glass and backing and applying the full formula (3) with glass as layer 1 and the helium film as layer2.

In Fig. 6b the result is compared with the experimental spectrum. Now simulation and experiment agree even below 400 cm^{-1}. Due to the $1/\sqrt{\omega}$ dependence of the thermal diffusion length μ_{therm} the insertion of the small helium film has no influence on the simulated spectrum above 500 cm^{-1} since above that frequency μ_{therm} is substantially smaller than the sample thickness d_1. For comparison Fig. 6c shows how the relative photoacoustic signal changes if we

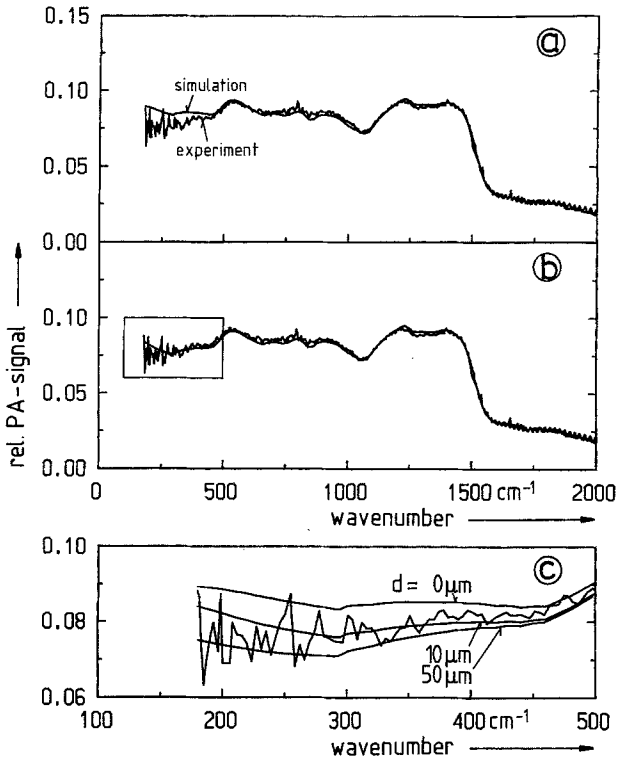

Fig. 6a–c. Experimental and simulated spectra of the glass sample. (a) The glass sample was assumed to be lying directly on the brass backing, and formula (4) was used. (b) Now in the simulation a thin helium layer ($d=10$ μm) was inserted between the sample and the backing using formula (3). (c) Magnified view of the region indicated by the box in (b). The measured spectrum is compared with the simulated spectra obtained for different thicknesses of the helium film ($d=0$ μm, 10 μm, 50 μm)

assume different values for the thickness of the helium film (0 μm, 10 μm, and 50 μm).

We want to stress that the only parameter involved is the thermal conductivity of carbon black. But its value is obtained here once and for all by fitting the glass simulation to the experiment, and is used throughout the simulations.

3.2. *Properties of Carbon Black*

To simulate the carbon black spectrum we had to know the optical and thermal properties of this powder.

The high optical integral absorption in carbon black is due to the internal structure which resembles that of a sponge consisting of a strongly absorbing material. The penetrating light is already absorbed in a small surface layer. We simulated that by assuming a rather high effective optical absorption coefficient K_{eff} and a vanishing reflectance, which was verified by measuring the diffuse reflectance. For K_{eff} we can assume a value such that the related optical penetration depth $d_{\text{opt}} \ll \mu_{\text{therm}}$. Rosencwaig and Gersho have already shown that in this special case the photoacoustic signal is independent of the optical absorption coefficient [1].

The density of carbon black could easily be measured:

$$\varrho_{\text{cb}} \approx 0.175 \frac{\text{g}}{\text{cm}^3}.$$

By comparing this result with the density of solid graphite we got the mass fraction f of carbon in helium for the carbon powder. The specific heat capacity then was obtained by averaging the values for carbon and helium:

$$c_{\text{cb}} = f c_{\text{carbon}} + (1-f) c_{\text{helium}},$$

where c_{cb}, c_{carbon}, and c_{helium} denote the respective mass specific heat capacities. With this formula we got

$$c_{\text{cb}} \approx 733 \frac{\text{J}}{\text{kg} \cdot \text{K}}.$$

We mentioned above that to fit the simulated relative photoacoustic spectrum to a measured one we used λ_{cb} as the only fit parameter. The value obtained was

$$\lambda_{\text{cb}} \approx 0.145 \frac{\text{W}}{\text{m} \cdot \text{K}}.$$

By this method it is possible to determine the thermal conductivity of an unknown highly absorbing sample from a photoacoustic rapid scan Fourier spectrum.

Acknowledgements. We wish to thank B. Harbecke and W. Theiß for helpful discussions.

References

1. A. Rosencwaig, A. Gersho: J. Appl. Phys. **47**, 64 (1976)
2. P. Hess, J. Pelzl: Springer Ser. Opt. Sci. Vol. **58** (Springer, Berlin, Heidelberg 1988)
3. G. Busse, B. Bullemer: Infrared Phys. **18**, 631 (1978)
4. S. Perkowitz, G. Busse, in: *Electromagnetic Waves in Matter*, Vol. 16, Part III (Academic, London 1986)
5. M.A. Afromowitz, P.S. Yeh, S. Yee: J. Appl. Phys. **48**, 209 (1977)
6. P. Grosse: *Freie Elektronen in Festkörpern* (Springer, Berlin, Heidelberg, New York 1979), p. 248
7. B. Harbecke: Appl. Phys. B **39**, 165 (1986)
8. P. Grosse, B. Harbecke, B. Heinz, R. Meyer, M. Offenberg: Appl. Phys. A **39**, 257 (1986)